ACS OMEGA

Open Access

http://pubs.acs.org/journal/acsodf

Article

Mussel-Inspired *In Situ* Photodynamic Antibacterial Coating for Postoperative Management of Artificial Corneas

Muchen Dong,*,# Qingdong Bao,# Ruyu Feng, Suxia Li, Xin Wang, Chunxiao Dong, Guangwei Li, and Weiyun Shi*

Cite This: *ACS Omega* 2025, 10, 3676−3690

Read Online

ACCESS | Metrics & More | Article Recommendations | Supporting Information

ABSTRACT: Artificial corneal (AC) implants offer hope to millions with corneal blindness, including 5 million in China. Titanium is one of the materials commonly used in the fabrication of artificial corneal scaffolders because of its light texture, high mechanical properties, and high biosafety. However, postoperative bacterial infections, especially from *Pseudomonas aeruginosa* and *Staphylococcus aureus* (*S. aureus*), remain a significant challenge due to the bioinert nature of titanium materials, leading to high infection rates. In this study, we introduce an innovative *in situ* photodynamic coating technology designed to manage postoperative infections in artificial corneas. Inspired by mussel adhesive proteins, this coating employs a composite of APTES-TA formed by Schiff base and Michael addition reactions between 3-aminopropyltriethoxysilane (APTES) and tannic acid (TA), integrated with the bacterial targeting capabilities of 4-carboxyphenylboronic acid (CPBA) and the photo-Fenton activity of FeOOH (iron(III) hydroxide). The design of the AC@APTES-TA-CPBA-FeOOH coating leverages the dynamic boronate ester bonds, which interact specifically with bacteria in tears, effectively capturing them on the surface of the artificial cornea. The coating exhibits a photocatalytic Fenton-like effect, which confers it with an exceptional bactericidal efficiency of over 99% *in vitro*. Furthermore, it demonstrates excellent protective functionality for mouse corneas *in vivo* experiments.

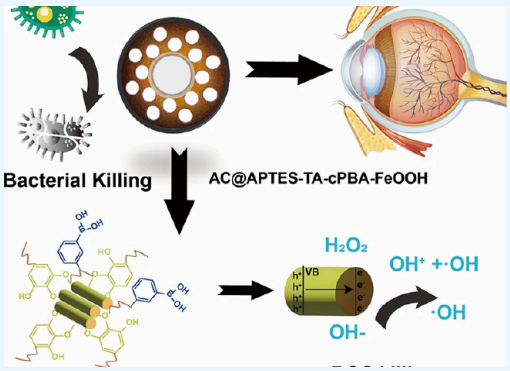

1. INTRODUCTION

Artificial corneal (AC) implants are a crucial advancement in medical technology, providing an alternative treatment for patients at risk of vision loss due to corneal diseases.[1] According to the World Health Organization (WHO), approximately 60 million people worldwide suffer from corneal blindness, with China accounting for about 5 million of these cases.[2,3] If the retina and optic nerve function are basically normal, artificial cornea becomes an important means to restore vision for patients with high-risk corneal transplantation, such as ocular burns, whose conventional penetrating corneal transplantation is difficult to succeed.[4] Titanium is one of the materials commonly used in the fabrication of artificial corneal scaffolders because of its light texture, high mechanical properties and high biosafety.[5] However, such implants often face challenges, particularly with bacterial infections that limit their broader clinical use.

Postoperative complications include infections due to gaps at the implantation site, which allow bacteria such as *Pseudomonas aeruginosa (P. aeruginosa)* and *Staphylococcus aureus (S. aureus)* to enter, significantly increasing infection risks.[6] The rate of postoperative infectious endophthalmitis, a severe complication, is around 6.1%.[7] This high infection rate is attributed to the bioinert properties of the titanium-based materials used, which support bacterial adhesion and growth.[8] Despite antibiotics, the infection rate after implantation remains high at nearly 3%, partly due to bacterial accumulation on the implant surface.[9]

To combat these issues, surface modification techniques such as antibacterial coatings inspired by mussel have been developed. These coatings utilize mussel protein sequences that exhibit strong bacterial adhesion and antimicrobial properties.[10−14] They function through contact-mediated and oxidative killing mechanisms, significantly enhancing the effectiveness of artificial corneas against infections.[15] Therefore, this contact-based oxidation bactericidal strategy can be an effective candidate for the surface modification strategy of artificial cornea.

Photodynamic therapy (PDT), which uses light-activated photosensitizers to generate reactive oxygen species (ROS) that kill bacteria, fungi, and viruses effectively.[16] This includes

Received: September 22, 2024
Revised: December 27, 2024
Accepted: January 15, 2025
Published: January 24, 2025

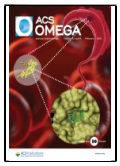

the use of polyphenol-metal complexes that form strong chelating networks capable of producing substantial ROS through the photo-Fenton effect, enhancing antimicrobial efficacy.[17] Photosensitizers activated by light of specific wavelengths generate ROS, which can destroy various biomolecules within cells, including proteins, lipids, and nucleic acids, effectively killing bacteria, fungi, and viruses. Researchers have explored various phototherapeutic nanomaterials for antibacterial applications, such as pyridyl-porphyrin based, thiazine dye based, carbon-based, and polymer-based nanomaterials.[8,18−21] Among these, polyphenol-metal complexes have attracted increasing attention due to their unique antibacterial potential. In particular, the emerging field of polyphenol-metal coordination chemistry offers new approaches for functionalizing implant materials.[22] For instance, tannic acid (TA), containing catechol or galloyl groups, can form strong chelating polyphenol-metal coordination networks with various metal ions (M). These networks, upon mineralization, can produce substantial amounts of ROS through the photo-Fenton effect, thereby enhancing their antimicrobial efficacy.[17] Since Caruso et al. first reported the one-step rapid membrane assembly technique for TA-M coordination complexes, polyphenol-metal coordination chemistry has been successfully applied to the antimicrobial design of implant surfaces.[23] However, the short half-life of reactive oxygen radicals limits their effective duration, particularly in open application scenarios such as the eye, where it is challenging to precisely control the action of ROS within the infected area.[24] Therefore, enhancing the capture capability of artificial corneas for planktonic bacteria becomes particularly critical. This not only reduces the distance between ROS and bacterial cells, thereby increasing the bacterial killing efficiency, but also effectively lowers the risk of postoperative infections.

The dynamic noncovalent bonds of boronic esters provide a robust molecular theoretical basis for the development of bacterial capture technologies in artificial corneas. Phenylboronic acid (PBA), have shown promise in bacterial capture technologies.[22]

CPBA binds specifically to diol-containing saccharides found in the cell walls of bacteria, enhancing the capture, and killing of bacteria on the corneal surface. This reduces the distance between ROS and bacterial cells, increasing the bactericidal efficacy and lowering postoperative infection risks.

In this study, we introduce an innovative in situ photodynamic coating technology designed to manage postoperative infections in artificial corneas (Scheme 1). Inspired by mussel adhesive proteins, this coating employs a composite of APTES-TA as a base, integrated with the bacterial targeting capabilities of CPBA and the photo-Fenton activity of FeOOH (iron(III) hydroxide). The design of the AC@APTES-TA-CPBA-FeOOH coating leverages the dynamic boronate ester bonds, which interact specifically with bacteria in tears, effectively capturing them on the surface of the artificial cornea. Once bacteria are captured, the FeOOH component within the coating, under exposure to sunlight or visible light, catalyzes the production of ROS, which possess potent bactericidal properties capable of rapidly eliminating the captured bacteria, thereby effectively preventing. In addition, hydroxyl radicals have a short half-life and cannot freely pass through cell membranes. They only exist on the eye surface. Antioxidants such as ascorbic acid, lactoferrin, uric acid and cysteine exist in tears, which can protect the eye surface from the damage of some free radicals. It can control the risk of infection following

Scheme 1. Schematic Illustration of the Application Scenarios, Fabrication Process, and Antibacterial Mechanism of Artificial Corneas with *in Situ* Photodynamic Antibacterial Coating.

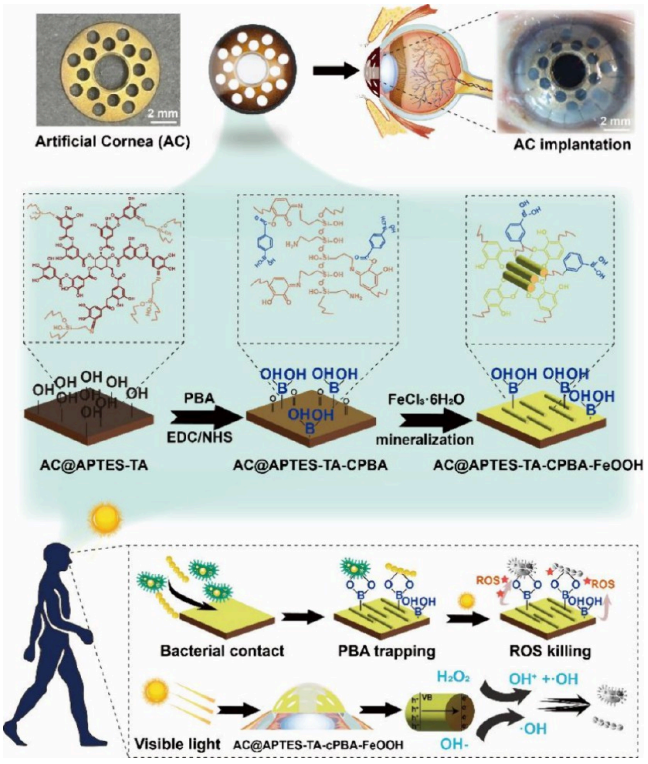

corneal implantation without damaging the normal physiological environment of the eye.[25] Overall, the AC@APTES-TA-CPBA-FeOOH coating technology provides an innovative strategy for preventing and controlling infections postartificial corneal implantation, showcasing the immense potential of solving clinical problems through advancements in materials science and biomedical engineering.

2. MATERIALS AND METHODS

2.1. Materials. Artificial corneas were purchased from Guangdong Jiayue Meishi Biotechnology Co., Ltd. Tannic acid (TA, > 99%), 3-Aminopropyltriethoxysilane (APTES, > 99%), 1-ethyl-3-(3-dimethylaminopropyl) carbodiimide (EDC, > 99%), N-hydroxysuccinimide (NHS, > 99%), Iron(III) chloride hexahydrate ($FeCl_3·3H_2O$), Fetal Bovine Serum (FBS), and antibiotics (penicillin-streptomycin) were purchased from Sinopharm Chemical Reagent Ltd. (Shanghai, China). 4-Carboxyphenylboronic acid (CPBA, 97%), and Tris(hydroxymethyl)aminomethane (>99%) were purchased from Shanghai Maclin Biochemical Technology Co., LT. Phosphate buffer solution PBS was purchased from Shandong Sikejie Biotechnology Co., Ltd. NaOH (95%) was purchased from Shandong Keyuan Biochemical Co., Ltd. H_2O_2 (3%) was purchased from Xiamen Emimani Biotechnology Co., Ltd. Bacterial viability assay kit was purchased from Abcam Ltd. (America). LIVE/DEAD cell viability assay kit was purchase from Merck KGaA (Germany). Trypsi and SYTOX Green nucleic acid dye (>99%) were purchased from Thermo Fisher Scientific (America). *Staphylococcus aureus* (*S. aureus*, KCTC 1621) and *Pseudomonas aeruginosa* (*P. aeruginosa*, PKE117) were purchased from China General Microbiological Culture

https://doi.org/10.1021/acsomega.4c08700
ACS Omega 2025, 10, 3676−3690

Collection Center (CGMCC). All chemical reagents and solvents were obtained from commercial suppliers and used without further purification.

2.2. Preparation and Characterization of AC@APTES-TA-CPBA-FeOOH. *2.2.1. Surface Alkali Treatment of Artificial Corneas.* Artificial corneas were subjected to surface alkali treatment by initially immersing them in anhydrous ethanol followed by ultrasonic cleaning for 15 min. The samples were then dried and subsequently immersed in a 2 M NaOH solution and heated at 80 °C for 2 h. Post-treatment, the corneas were thoroughly cleansed with ultrapure water and anhydrous ethanol via ultrasonic cleaning, then dried and reserved for further use.

2.2.2. Preparation of APTES-TA Coating on Artificial Corneas. For the preparation of the APTES-TA coating on artificial corneas, we dissolve Tannic acid (TA) and 3-Aminopropyltriethoxysilane (APTES) separately in a Tris buffer solution (pH 8.5) to achieve concentrations of 2 mg/mL for TA and 10 mg/mL for APTES. These solutions are then mixed in equal volumes to ensure a balanced reaction between TA and APTES. The mixture is gently. The alkali-treated artificial corneas (AC−OH) were immersed in this solution, wrapped in aluminum foil, and placed on a constant temperature shaker for 24 h at 37 °C and 180 rpm. Following the reaction, the samples were cleansed with ultrapure water and anhydrous ethanol using ultrasonic cleaning, then dried and reserved.

2.2.3. CPBA Grafting. CPBA (0.09 g) and EDC (0.07 g) were dissolved in 60 mL anhydrous ethanol. The AC@ APTES-TA was then immersed in this solution and reacted at 37 °C and 180 rpm for 1 h. Subsequently, NHS (0.01 g) was added to mixed solution, and the reaction continued under the same conditions for an additional 24 h. After completion, the samples were cleansed with ultrapure water and anhydrous ethanol using ultrasonic cleaning, then dried and reserved.

2.2.4. Surface Mineralization. $FeCl_3{\cdot}3H_2O$ (0.48 g) was dissolved in a mixture of 30 mL HCl (0.01M) and 60 mL ultrapure water. The AC@ APTES-TA-CPBA was immersed in this solution, wrapped in aluminum foil, and reacted in an oven at 60 °C for 24 h to obtain AC@ APTES-TA-CPBA@ FeOOH. Following the reaction, the samples were similarly cleansed and dried for further use.

2.2.5. Characterization. The morphological characteristics of the samples were observed using a field emission scanning electron microscope (FESEM, Hitachi S4800, Japan). Surface elemental analysis was conducted using X-ray photoelectron spectroscopy (XPS, PerkinElmer, Waltham, MA). Chemical bonding was identified through Fourier-transform infrared spectroscopy (FTIR, Nicolet 6700). The optical absorption properties were assessed using UV−visible spectroscopy (UV−vis, UV 2450, Shimadzu, Japan). Photocatalytic performance of the coatings was evaluated using a photoluminescence spectrometer (FLS920, Edinburgh Instruments) equipped with a Xe lamp (450 W, 325 nm) as the excitation source. The surface potentiometer (SurPASS3, Austria) was used to measure the surface potential of the sample before and after modification.

2.3. Hydrophilicity. To evaluate the wettability of the surface coatings on artificial corneas, a DSA100 dynamic water contact angle (WCA) instrument was utilized. This instrument precisely measures the angle formed between a liquid and a solid surface, which reflects the surface's hydrophilic or hydrophobic characteristics. Initially, the samples were thoroughly dried in a controlled environment and carefully placed on the testing stage of the WCA instrument. Subsequently, the droplet volume was set to 2 μL to ensure the accuracy and reproducibility of the measurements. Once the droplet formed and appeared as a perfectly smooth spherical shape, the measurement process was initiated. To enhance the reliability of the data, three independent contact angle measurements were conducted at different locations on each sample. The average of these measurements was calculated to determine the final wettability parameters.

2.4. Durability. The dissolution rate and longevity of artificial corneas are pivotal for evaluating their safety and efficacy. Surface coatings are a focus of research to improve these properties. This study investigates the durability of variously coated artificial corneas through experimental characterization.AC−OH (surface-alkalized Ti metal), AC@ APTES-TA (APTES-grafted), AC@APTES-TA-CPBA (CPBA-modified), and AC@ APTES-TA-CPBA-FeOOH (in situ mineralized)— in artificial tear fluid mimicking physiological conditions. Dissolution was monitored by sampling and testing ultraviolet absorption spectroscopy every 7 days.

2.5. Photocatalytic Performance Measurement. This experiment aimed to evaluate the photocatalytic activity of modified artificial corneas by degrading various dyes in water. A 500 W xenon lamp equipped with a 420 nm cutoff filter served as the visible light source. Before irradiation, the artificial corneas were immersed in a dye-containing aqueous solution (25 mL, concentration of 20 mg/L, pH adjusted to 3) and agitated in the dark for 30 min to achieve adsorption−desorption equilibrium.

Before the experiment commenced, the initial concentration of the dye solution (C0) was recorded. H_2O_2 was then added to the solution to achieve a final concentration of 9.8 mM, initiating the photo-Fenton reaction. During the visible light irradiation, 1 mL samples were periodically extracted from the solution, diluted to 3 mL, and analyzed to measure changes in dye concentration (Ct). This monitoring allowed for the calculation of dye degradation efficiency. By comparing degradation efficiencies under different conditions, the photocatalytic performance of the artificial corneas could be assessed, providing insights into their effectiveness in catalytic processes under simulated environmental conditions.

2.6. *In Vitro* Antimicrobial Performance Characterization. For this study, *P. aeruginosa* and *S. aureus* were prepared with the concentration of 10^9 CFU/mL. Bacterial suspension with a volume of 500 μL was applied to the surfaces of different experimental groups, including AC−OH, AC@APTES-TA, AC@APTES-TA-CPBA, and AC@APTES-TA-CPBA-FeOOH. These samples were incubated for 1.5 h to simulate bacterial infection. After incubation, 150 μL of 0.5 M H_2O_2 solution was added to each group. The samples in the phototreatment group were then exposed to blue light (20 W, 420−430 nm wavelength) for 30 min, while the control group was kept in darkness for the same duration. After incubation, each sample was gently rinsed three times with 2 mL of PBS buffer. This was done to remove any loosely adherent bacteria or debris. The gentle nature of the rinsing was to prevent any disruption to the surface coating while ensuring that nonadherent bacteria were removed. Postincubation, the LIVE/DEAD BacLight Bacterial Viability Kit from ThermoFisher was used according to the manufacturer's instructions by adding SYTO-9/PI dyes to the culture systems. After a 20 min incubation, the samples were washed three times with PBS

https://doi.org/10.1021/acsomega.4c08700
ACS Omega 2025, 10, 3676−3690

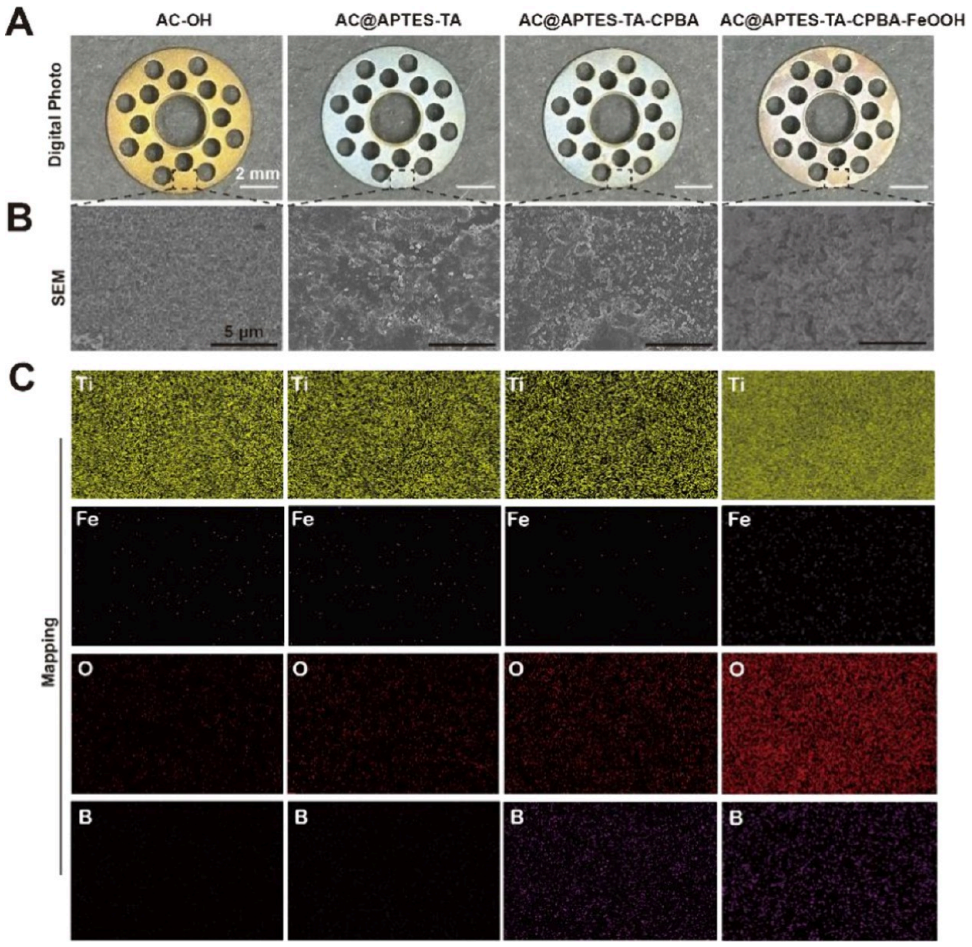

Figure 1. (A) The surface color of the artificial cornea evolves with the progression of modifications, (B) SEM photos, and (C) Mapping of AC−OH, AC@APTES-TA, AC@APTES-TA-CPBA, and AC@APTES-TA-CPBA-FeOOH.

buffer to remove unbound dye. The treated bacteria were then observed under a Zeiss LSM 880 confocal laser scanning microscope (CLSM) manufactured in Germany, to analyze their viability.

Sterilization rate of bacteria on the surface of artificial cornea was also assessed. Bacterial suspensions (10^9 CFU/mL) were applied to the surfaces of the experimental groups and incubated for 3 h. After incubation, the surfaces were thoroughly rinsed with 2 mL of PBS buffer, and 100 μL of the rinse was used for plating. Agar plates were then incubated for 24 h, followed by colony counting to quantitatively analyze the bactericidal effects. By comparing the colony-forming units (CFU) across different experimental groups, the antibacterial performance of the artificial corneal surfaces was evaluated.

2.7. Cytotoxicity Assessment. *2.7.1. Cell Viability Assessment.* Before plating, Human Corneal Epithelial Cells (HCEC) were washed, digested, and centrifuged. Cells were resuspended in 4 mL of complete culture medium and counted. Based on the cell concentration, they were diluted to 5×10^4 cells/mL. Three 96-well plates were prepared, with 0.1 mL of PBS added to the outer wells to create a humidity barrier. Cell suspension was then distributed into the 96-well plates, setting up blank wells, control wells, and test wells with five replicates each. Medium without cells was added to the blank wells, while cell suspension was added to control and test wells. Plates were gently shaken for even distribution and then placed in a 37 °C incubator to form a semiconfluent monolayer.

2.7.2. Artificial Cornea Sample Pretreatment and Coculture. Artificial cornea samples from different experimental groups were sterilized under UV light for 3 h on a clean bench. After sterilization, variously coated artificial corneas were immersed in 10 mL of complete culture medium and sealed. They were then placed on a shaker at 60 rpm for 4 h to allow leachables to release. The leachate was then sterilized under UV light for 1 h. After removing the original medium from the 96-well plates, it was replaced with an equal volume of sterilized gel leachate for coculture over 24 h.

2.7.3. Cell Viability Evaluation. To assess cell viability, the Cell Counting Kit-8 (CCK-8) assay was employed. In a light-protected environment, CCK-8 reagent was mixed with the medium at a 1:9 ratio to prepare the CCK-8 working solution. After aspirating the medium from the wells and gently washing the cells twice with fresh medium to remove residual medium, 100 μL of CCK-8 working solution was added to each well. The treated 96-well plate was then incubated for 2 h in the dark. Postincubation, the absorbance of each well was measured at 450 nm using a spectrophotometer to evaluate the relative cell viability

2.8. In Vivo Experiments. In this study, we utilized a C57BL/6 mouse model to simulate corneal damage and subsequent infection processes. Initially, surface anesthesia was applied to the mice's eyes using a drop of 0.5% proparacaine

https://doi.org/10.1021/acsomega.4c08700
ACS Omega 2025, 10, 3676−3690

hydrochloride. A corneal epithelial scraper was then used to randomly create injuries on the corneas of the mice to mimic corneal damage. To simulate the application of artificial corneas, circular titanium discs treated differently (CA−OH, CA@APTES-TA, CA@APTES-TA-CPBA, CA@APTES-TA-CPBA-FeOOH) were placed on the damaged corneal areas.

Subsequently, a microliter syringe was used to slowly inject 4 μL of a *P. aeruginosa* suspension (10^9 CFU/mL) at the interface between the titanium disc and the cornea to simulate bacterial infection. Additionally, to replicate oxidative stress conditions, 9.8 mM of H_2O_2 was added. The mice were divided into two groups: one subjected to 30 min of visible light exposure (30 min), and the other cultured in darkness. Corneal cloudiness was monitored by photographing the mice's corneas every 24 h. Initial photographs were taken using a slit lamp microscope (Model: AX7000297) before the experimental procedures. For clear imaging, the light was adjusted to white, magnification set to 25 × , and both angle and slit width were fine-tuned to ensure the corneal reflection point was centered on the pupil. Subsequent photographs were taken every 24 h over three consecutive days. Each photograph was meticulously cataloged by date, mouse number, and whether it was the left or right eye. After the third set of photographs, the mice were euthanized by cervical dislocation, and their eyeballs were harvested. After removing extraocular muscles and optic nerves, the eyeballs were embedded in 1.5 mL of OCT compound (Brand: SAKURA), labeled, and numbered before being stored at −80 °C for further analysis.

2.9. Immunohistochemical Analysis. For histological examination, eyeball tissues embedded in OCT were removed from 1.5 mL centrifuge tubes. The tissues were then placed on the cryostat's freezing stage and fix the sample directly to the sample holder. The holder was attached to the cryostat's sample stage to ensure stability during slicing. The cutting blade was then mounted on the blade holder and fixed in place. The initial slicing thickness was set at 100 μm on the control panel, and the wheel was turned to remove excess OCT until the tissue was fully exposed. Once exposed, the slicing thickness was adjusted to 8 μm for finer cuts. During the slicing process, intact slices were selected and mounted onto the front of glass slides. Finally, tissue-mounted slides were stained with Hematoxylin and Eosin (H&E) for microscopic examination of tissue morphology.

2.10. Statistical Analysis. The statistical analysis and graphical presentation of experimental data were done by one-way analysis of variance (one-way ANOVA), and all data were presented as the means and standard deviations, indicated as the mean ± SD.

3. RESULTS AND DISCUSSION

3.1. Preparation and Characterization of AC@APTES-TA-CPBA-FeOOH. The application of layer-by-layer self-assembly technology has facilitated progressive modifications in the surface properties of artificial corneas, manifesting not only in macroscopic changes, such as color alterations, but also in microscopic compositional and structural transformations. TA oxidizes to quinone under weak base conditions, and APTES hydrolyzes to chain segment compounds containing amino groups. Michael addition and Schiff base react between the two to form TA-APtes coating, and interact with AC surface through hydrogen bonding. A disordered nanospherical structure (100−300 nm) is formed and uniformly distributed on the surface of the artificial cornea to form AC@APTES-TA. The carboxyl group of CPBA forms borate bond with the hydroxyl group of tannic acid to form AC@APTES-TA-CPBA on APTES-TA. Fe3+ forms AC@APTES-TA-CPBA-FeOOH by chelating coordination mineralization with TA. As depicted in Figure 1A, the surface color of the artificial cornea evolves with the progression of modifications, culminating in a specific brownness. As shown in Figure 1B, following alkali treatment, the AC−OH surface exhibits a porous and rough microstructure with pore sizes ranging between 100−300 nm (Figure S3). The corrosive action of NaOH increases the −OH content on the AC surface, thereby enhancing its compatibility with subsequent modification techniques. The integration of TA introduces catechol groups $(-OH)_2$, which, upon oxidation (=O), can form dynamic covalent Schiff base (-N = C−) linkages with the amine groups (−NH2) on APTES and interact with AC surfaces through hydrogen bonding, resulting in the formation of disordered nano spherical structures (100−300 nm). These structures are uniformly distributed over the artificial cornea surface. This reaction is indeed fundamental to the successful application of the APTES-TA coating on the artificial cornea surface, as it ensures a robust attachment and creates a platform for further modifications.To further elaborate, the Schiff base formation is a dynamic process that allows for the reversible linkage between the aldehyde groups from the oxidized catechol structures of tannic acid and the primary amine groups of APTES. This dynamic nature is advantageous for the coating's adaptability and responsiveness in various physiological conditions.

Exposed amine groups on the APTES-TA coating serve as reactive sites for the introduction of CPBA. Catalyzed by NHS and EDC, the phenylboronic acid groups covalently bond to the APTES-TA surface. This step not only enhances the adhesion of the coating to the surface but also strengthens various physicochemical mechanisms such as $\pi-\pi$ stacking and conformational rearrangements induced by oxidative side-chain isomerization of catechol, thereby ensuring robust attachment of the APTES-TA-CPBA coating to the artificial cornea surface. Ultimately, in situ mineralization of FeOOH (iron(III) hydroxide) nanorods occurs on the APTES-TA-CPBA coated substrate through a hydrolysis reaction. In this process, the APTES-TA-CPBA layer plays a critical role in capturing Fe ions through chelation with catechol, forming nucleation sites that not only promote the mineralization process but also aid in the stabilization of the coating, resulting in the formation of a disordered distribution of nanospherical morphologies on the artificial cornea surface. The NaOH treatment etches away impurities and possibly breaks some surface bonds, leading to an increase in surface roughness. This roughness, along with the introduction of additional −OH groups, enhances the surface's reactivity. The increased surface roughness and the presence of more −OH groups improve the compatibility of the AC surface for subsequent chemical modifications. This oxidation step is crucial for the formation of the TA-APTES coating, as it allows for the creation of dynamic covalent Schiff base linkages with the amine groups on APTES, enhancing the coating's stability and functionality on the artificial cornea surface.

The surface elemental composition of the artificial cornea also underwent significant changes, as illustrated in Figure 1C. Following alkali treatment, the surface of the artificial cornea exhibited a pronounced presence of Ti elements, constituting 98% of the surface, while the signals for O were relatively weak,

https://doi.org/10.1021/acsomega.4c08700
ACS Omega 2025, 10, 3676−3690

recorded at 2%. At this stage, elements such as Fe and B were not detected. With the sequential introduction of APTES and CPBA, the chemical composition of the artificial cornea surface was considerably enriched. The modification with APTES-TA notably increased the presence of hydroxyl (−OH), siloxane (−Si-O−), and carbonyl (-C = O−) groups on the surface. Tannic acid's inherent phenolic groups, including catechol moieties, play a pivotal role in the surface modification process due to their reactivity. The addition of CPBA further introduced boron (-B-) bonds, resulting in increased contents of O and B to 13% and 2% respectively. Subsequent in situ mineralization processes, through hydrolysis reactions led to the formation of FeOOH nanoparticles on the surface of APTES-TA- CPBA. This step significantly enhanced the surface concentration of Fe on the AC, with the detected percentage rising to 5% (Table 1). This comprehensive

Table 1. Elemental Analysis of AC−OH, AC@APTES-TA, AC@APTES-TA-CPBA, and AC@APTES-TA-CPBA-FeOOH

Type of AC	Ti (%)	O (%)	B (%)	Fe (%)
AC−OH	98	2	0	0
AC@APTES-TA	90	10	0	0
AC@APTES-TA-CPBA	85	13	2	0
AC@APTES-TA-CPBA-FeOOH	70	20	5	5

alteration in surface chemistry not only reflects the layered modifications but also underscores the potential for tailored functionalization in biomaterial applications.

During the surface modification process of the AC, significant alterations were observed in the surface charge, as evidenced by changes in the zeta potential (Figure S1). The AC−OH surface exhibited electronegativity, with a measured zeta potential of −5 mV. The introduction of the APTES-TA coating led to an increase in the zeta potential to 8.3 mV, a change primarily attributed to the presence of amine groups ($-NH_2$) within the APTES molecules. Subsequently, the hydroxyl (−OH) functional groups of the CPBA molecules further reduced the surface charge density of the coating (3.6 mV). Ultimately, the in situ mineralization process, resulting in the formation of FeOOH, endowed the AC with a near-neutral surface charge (0.5 mV). This adjustment is anticipated to positively influence the biocompatibility of the coating and enhance its performance in subsequent biological applications. This progression underscores the critical role of controlled surface charge modifications in tailoring the interface properties of biomaterials for optimized interactions in a physiological environment.

To further analyze the AC@APTES-TA-CPBA-FeOOH, ATR-FTIR was employed (Figure S2). Compared to the unmodified AC, the modified AC@APTES-TA surface displayed new absorption bands. Notably, the peaks at 1100 and 1708 cm^{-1} can be attributed to the vibrational modes of the −Si-O-bond and -C = O bond, respectively. The CPBA spectrum showed increasingly broad and intense absorption peaks at 1200 cm^{-1}, likely due to the overlapping of different chemical bonds such as −Si-O- and -B-. A broad absorption peak observed at 3400 cm^{-1} was likely due to the stretching vibrations of −N-H bonds. Peaks at 3300 and 800 cm^{-1} are attributed to the stretching vibrations of O−H and Fe−O bonds in β-FeOOH, indicating successful coating formation. These findings were further corroborated by XPS data (Figure 2A and 2B). In the XPS analysis, the APTES-TA coating, the Si 2p peak was significantly enhanced. Within the APTES-TA coating, characteristic peaks at 286.1 eV for the C 1s peak, 401 eV for the N 1s, and 540.2 eV for the O 1s were observed, corresponding to the products of Schiff base and Michael addition reactions. On the surface of the APTES-TA coating, signals for Fe 2p and B 1s peaks (724.2 and 201.1 eV) were not overserved. However, APTES-TA-CPBA showed the obvious peak of B 1s at 198.5 eV, due to the introduction of CPBA. Finally, signals at 724.2 and 710.8 eV correspond to characteristic peaks for Fe $2p^{1/2}$ and Fe $2p^{3/2}$, indicating that β-FeOOH nanoparticles have been successfully mineralized on the APTES-TA-CPBA coating. Therefore, these results confirm the successful fabrication of the APTES-TA-CPBA-FeOOH on the surface of AC.

3.2. Hydrophilicity of AC@APTES-TA-CPBA-FeOOH. The operational conditions of AC in the ocular environment necessitate exemplary hydrophilicity, as they must maintain close contact with ocular tissues and operate within a highly hydrated environment. The hydrophilicity of the AC@APTES-TA-CPBA-FeOOH is characterized by measuring the water contact angle, a critical parameter for assessing the surface hydrophilicity of materials. As shown in Figure 3A and 3B, the alkali-treated artificial cornea AC−OH exhibited a water contact angle of 84°, indicating relatively weak initial hydrophilicity. However, when the surface is covered with APTES-TA, the water contact angle decreased to 47°, demonstrating a significant enhancement in hydrophilicity. This enhanced hydrophilicity is attributed to the chemical reaction between TA and APTES, which forms nanospherical structures enriched with hydrophilic groups on the surface of the AC.

Further, the introduction of CPBA into the coating increased the water contact angle to 70°, suggesting a reduction in hydrophilicity. This change could be due to the introduction of CPBA increasing the proportion of hydrophobic structures on the coating's surface. Finally, the in situ mineralization of FeOOH reduced the water contact angle to 20°, benefiting from the inherent excellent hydrophilicity of FeOOH. These variations not only reflect the impact of coating composition on hydrophilicity but also are of significant relevance for the biocompatibility and long-term stability of AC. By precisely controlling the chemical composition and structure of the coating, the hydrophilicity of artificial corneas can be optimized, thereby enhancing their performance in the ocular environment, and improving patient comfort. This strategic approach to surface engineering underscores the critical importance of surface properties in the successful integration and functionality of biomaterials within biological systems

3.3. Durability of the AC@APTES-TA-CPBA-FeOOH. The dissolution rate and longevity of artificial corneas are pivotal for evaluating their safety and efficacy. Surface coatings are a focus of research to improve these properties. This study investigates the durability of variously coated artificial corneas through experimental characterization. We submerged samples of artificial corneas with distinct surface treatments—AC−OH (surface-alkalized Ti metal), AC@APTES-TA (APTES-grafted), AC@APTES-TA-CPBA (CPBA-modified), and AC@APTES-TA- CPBA-FeOOH (in situ mineralized)— in artificial tear fluid mimicking physiological conditions. Dissolution was monitored by sampling and ultraviolet absorption spectroscopy every 7 days.

https://doi.org/10.1021/acsomega.4c08700
ACS Omega 2025, 10, 3676−3690

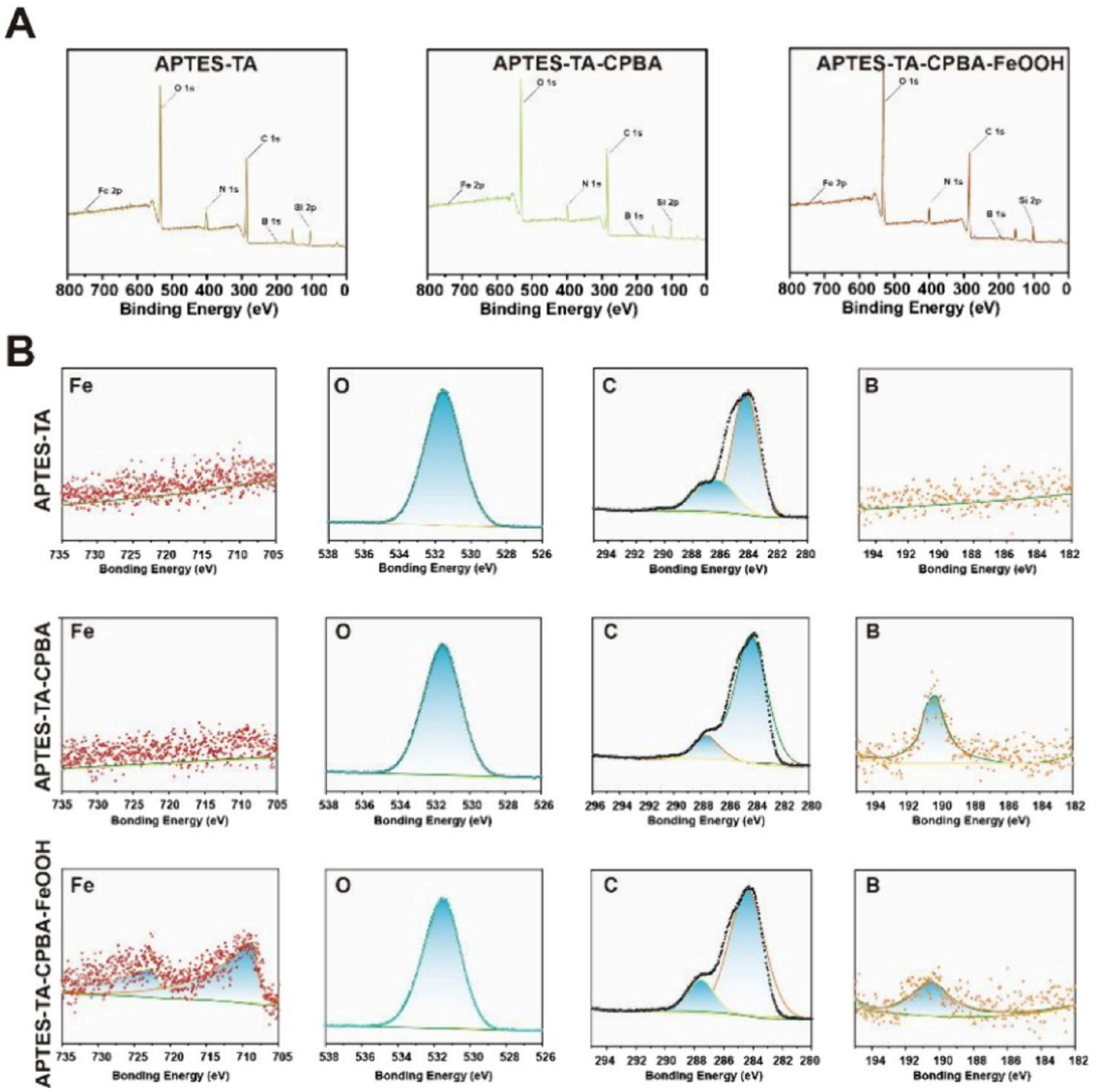

Figure 2. (A) XPS spectra of the APTES-TA, APTES-TA-CPBA, and APTES-TA- CPBA-FeOOH. (B) Fe, O, C, B core-level XPS spectra of the APTES-TA, APTES-TA- CPBA, and APTES-TA-CPBA-FeOOH.

Figure 3C illustrates that the AC@APTES-TA-CPBA-FeOOH sample showed negligible changes after 35 days, signifying superior stability. Conversely, the untreated AC−OH sample, as shown in Figure 3D, exhibited a low dissolution rate, expected due to its basic surface treatment. The AC@APTES-TA and AC@APTES-TA-CPBA samples, however, displayed a complete dissolution rate after 35 days, suggesting that their coatings are not stable enough for long-term immersion, likely due to hydrogen bonding and dynamic covalent interactions within the coatings. In contrast, the AC@APTES-TA-CPBA-FeOOH sample, which incorporated Fe ions, demonstrated enhanced stability through coordination and mineralization, maintaining its integrity under simulated physiological conditions. These results highlight the significance of coating stability and substrate bonding in artificial cornea design for long-term implant functionality. The exceptional performance of the AC@APTES-TA-CPBA-FeOOH sample offers a scientific basis for developing durable antibacterial artificial corneas, with potential for future clinical use.

3.4. Photocatalytic Performance of AC@APTES-TA-CPBA-FeOOH. APTES-TA-CPBA-FeOOH coating displays strong and broad absorption peaks within the visible light range of 400 to 600 nm (Figure S4). This suggests that the incorporation of FeOOH enables the AC to absorb more visible light, potentially enhancing its photocatalytic activity under visible light exposure (Figure 4A). To validate the photo-Fenton performance of the APTES-TA- CPBA-FeOOH, methylene blue (MB) was selected as a model organic pollutant. As shown in Figure 4B, the standard curve for MB was characterized. The degradation kinetics curve of MB under light exposure demonstrates near-complete degradation within 120 min (Figure 4C). As shown in Figure 4D, the concentration of MB decreased by 21.5% after 120 min in the absence of light, whereas the degradation efficiency reached 90% under visible light irradiation treated with AC@APTES-TA-CPBA-FeOOH. Concurrently, digital photographs of the MB concentration change over time also demonstrate that AC@APTES-TA-CPBA-FeOOH can transform the MB solution to an almost colorless state under light exposure (Figure 4E). Although H_2O_2 itself can decompose organic

https://doi.org/10.1021/acsomega.4c08700
ACS Omega 2025, 10, 3676−3690

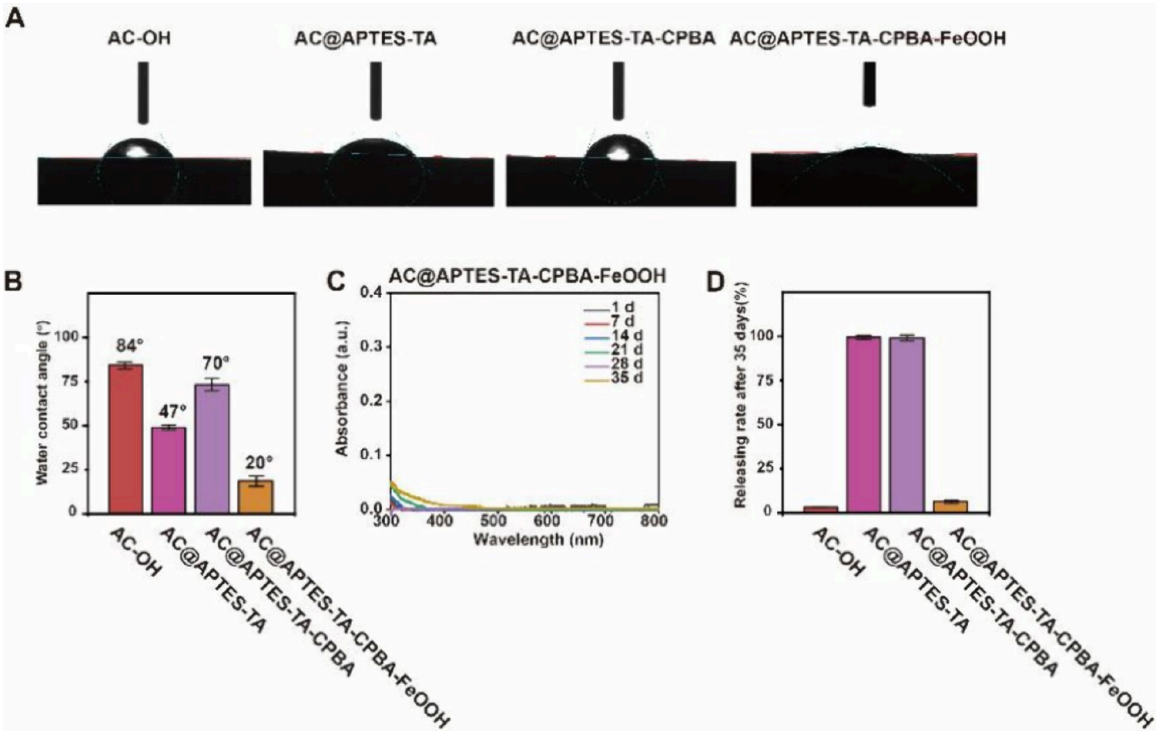

Figure 3. (A) Microscopic images and (B) measured data of the water contact angle in AC−OH, AC@APTES-TA, AC@APTES-TA-CPBA, and AC@APTES-TA-CPBA-FeOOH. (C) UV absorption spectral analysis of the eluate from AC@APTES-TA-CPBA-FeOOH over 30 days. (D) The elution rate of AC−OH, AC@APTES-TA, AC@APTES-TA-CPBA, and AC@APTES-TA-CPBA-FeOOH over 30 days.

substances, its use alone as a consumable would not sustain the rapid generation of hydroxyl radicals (•OH), leading to inefficient and costly treatment. The photocatalytic and Fenton catalytic actions within the APTES-TA-CPBA-FeOOH synergistically accelerate the production of •OH. The characteristic signal of hydroxyl radicals, indicated by four peaks with a ratio of 1:2:2:1 in the Electron Spin Resonance (ESR) spectrum (Figure 4F), further confirms the outstanding photo-Fenton catalytic activity of the coating. Specifically, β-FeOOH play a crucial role in the self-cleaning process. Under visible light, β-FeOOH generate photoinduced electrons (e−) and holes (h+), catalyzing the production of a significant amount of •OH. These highly oxidative hydroxyl radicals effectively eradicate bacteria adhering to the surface of the artificial cornea.

FeOOH (iron(III) hydroxide) plays a pivotal role in the photo-Fenton process due to its ability to act as a catalyst under light exposure. FeOOH can absorb photons and generate electron−hole pairs, where the photoinduced electrons reduce Fe(III) to Fe(II), and the holes (h+) can oxidize water molecules or hydroxide ions to generate hydroxyl radicals (•OH). The presence of H2O2 in the environment further enhances the generation of hydroxyl radicals. Fe(II) ions, produced either by the photoreduction of FeOOH or by the reaction of Fe(III) with H2O2, can react with H2O2 in a Fenton-like reaction to produce more hydroxyl radicals. This reaction is accelerated under light conditions due to the continuous regeneration of Fe(II) ions. The composite structure of APTES-TA provides a stable platform. CPBA, with its boronic acid groups, selectively captures bacteria, bringing them into close proximity with the FeOOH nanoparticles. This targeted adsorption reduces the distance between the bacteria and the reactive oxygen species, thereby increasing the bactericidal efficiency. The disordered nanospherical morphology of the coating, as characterized by SEM, creates a large surface area for the interaction between FeOOH, H2O2, and bacteria. This large surface area, combined with the light absorption properties of FeOOH, contributes to the efficient generation of hydroxyl radicals and the overall photocatalytic performance of the coating.

3.5. *In Vitro* Antibacterial Performance of AC@APTES-TA-CPBA-FeOOH. Following the modification with the APTES-TA-CPBA-FeOOH, the antibacterial properties of the artificial cornea were significantly enhanced. To assess this performance, SYTO-9 and propidium iodide (PI) fluorescent dyes were used for live/dead bacterial staining, where green fluorescence represents live bacteria and red fluorescence indicates dead bacteria. The antibacterial capability of the artificial cornea was initially characterized under dark conditions. As shown in Figure 5A, the unmodified AC−OH group displayed weak green fluorescence and no red fluorescence, indicating that the unmodified artificial cornea does not possess antibacterial properties. After the surface modification with APTES-TA, there was an increase in green fluorescence and a slight appearance of red fluorescence (accounting for 12%), which might be due to the introduced amine groups from APTES increasing the surface's positive charge, promoting bacterial adhesion, and potentially disrupting some bacterial cells.

With the further introduction of CPBA the intensity of green fluorescence on the artificial cornea surface continued to increase, but there was no significant change in red fluorescence (Figure 5B and 5C). This phenomenon might be attributed to the boronic acid groups in CPBAspecifically binding to bacterial cell walls, enabling the artificial cornea surface to actively capture bacteria, thus providing an effective

https://doi.org/10.1021/acsomega.4c08700
ACS Omega 2025, 10, 3676−3690

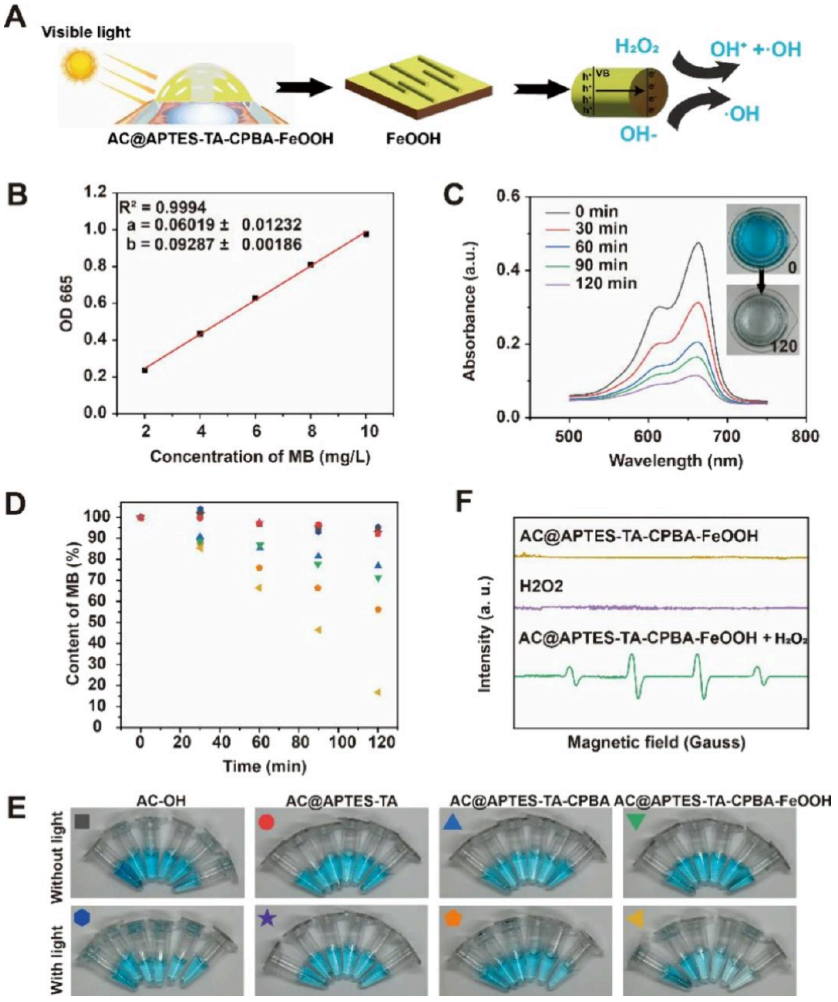

Figure 4. (A) Schematic illustration of antibacterial mechanism of AC@APTES-TA- CPBA-FeOOH. (B) Standard curve of MB. (C) UV Absorbance changes of MB treated with AC@APTES-TA-CPBA-FeOOH over 120 min. (D) Concentration changes of MB treated with AC−OH, AC@APTES-TA, AC@APTES-TA-CPBA, and AC@APTES-TA-CPBA-FeOOH. (E) Digital photos of MB concentration changes treated with AC−OH, AC@APTES-TA, AC@APTES-TA-CPBA, and AC@APTES-TA- CPBA-FeOOH. (F) The Electron Spin Resonance (ESR) spectrum of AC@APTES-TA-CPBA-FeOOH.

antibacterial barrier posteye implantation. Under dark conditions, AC@APTES-TA-CPBA-FeOOH did not exhibit significant antibacterial effects. However, upon light exposure, the AC@APTES-TA-CPBA-FeOOH coating exhibited excellent bactericidal performance, with extensive red fluorescence (100%) and disappearance of green fluorescence, indicating that nearly all bacteria were killed. This is attributed to the decomposition of H_2O_2 by FeOOH in the coating under photocatalytic conditions, generating a large amount of hydroxyl radicals. These radicals, under the targeted adsorption by CPBA, efficiently disrupt bacterial cell structures, achieving broad-spectrum bactericidal effects.

Further exploration of this bactericidal mechanism was conducted using SEM to characterize *Pseudomonas aeruginosa* and *Staphylococcus aureus*. As shown in Figure 5D, under dark conditions, *Pseudomonas aeruginosa* maintained its full rod-shaped structure. However, after light exposure, due to the destructive action of hydroxyl radicals, the cells of *Pseudomonas aeruginosa* showed significant fragmentation and collapse, with *Staphylococcus aureus* exhibiting similar destructive phenomena. This detailed characterization highlights the potent antibacterial capabilities of the APTES-TA-CPBA-FeOOH coating, particularly under light conditions, providing an effective strategy for enhancing the microbial resistance of biomaterials used in ocular applications

To quantitatively assess the antibacterial efficacy of the AC@APTES-TA-CPBA-FeOOH on artificial corneas, we employed the spread plate counting method (Figure 6A). The experimental results revealed that under dark conditions, the survival rates of *P. aeruginosa* were relatively high (60−100%) across all experimental groups, indicating limited antibacterial activity of the coating in the absence of light (Figure 6B and 6C). However, upon exposure to light, a dramatic reduction in bacterial viability was observed. The colony counts of *P. aeruginosa* in the groups treated with the AC@APTES-TA-CPBA-FeOOH coating decreased significantly, with survival rates plummeting to 1%, demonstrating the coating's high bactericidal efficiency under illuminated conditions. Similarly, *S. aureus* exhibited a high level of bacterial reduction, with the coating achieving an impressive 99% kill rate against both bacteria.

This marked antibacterial effect can be attributed to the targeted action mechanism within the coating system. The presence of CPBA groups in the coating enables specific

https://doi.org/10.1021/acsomega.4c08700
ACS Omega 2025, 10, 3676−3690

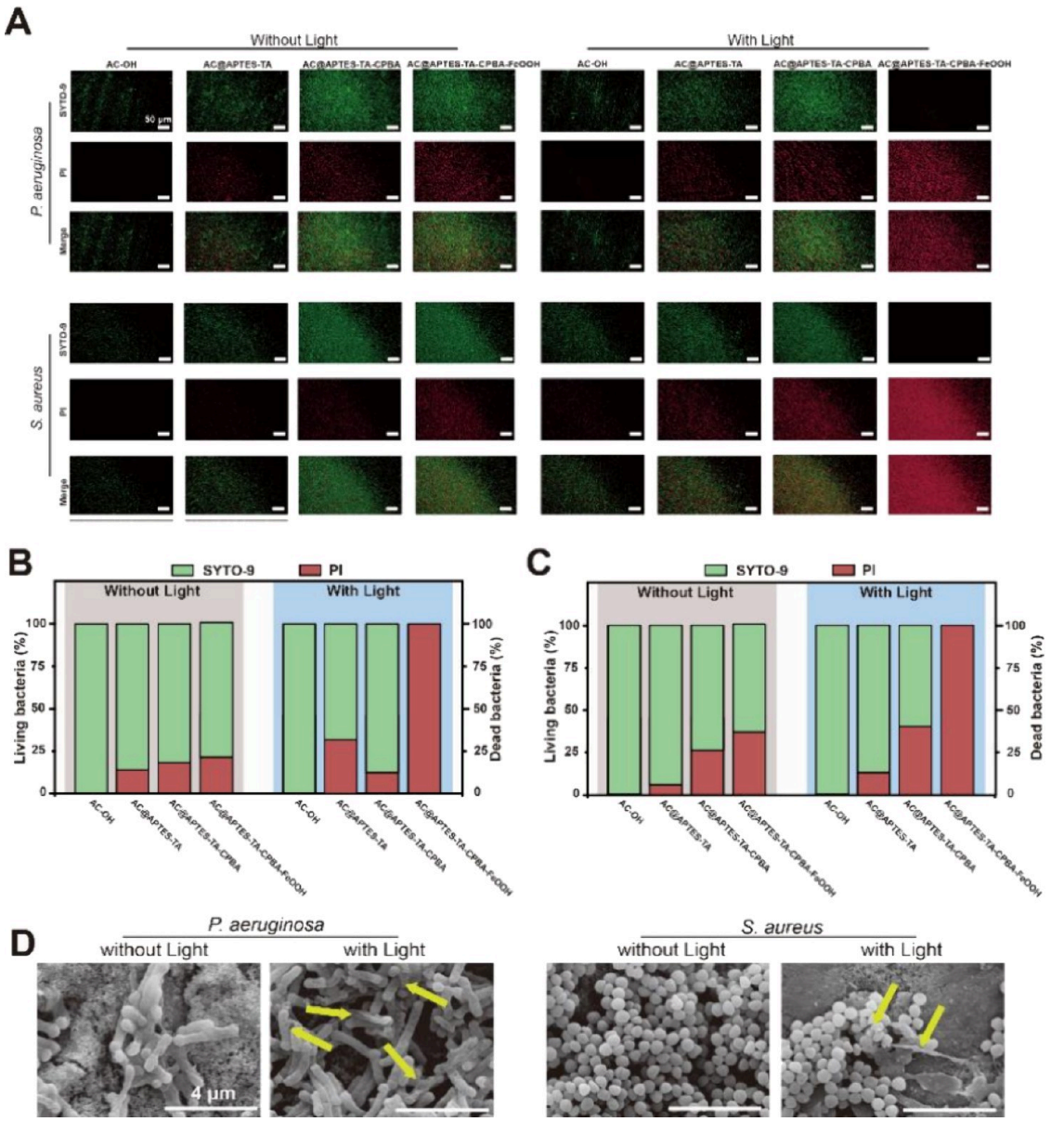

Figure 5. (A) Live/Dead staining of bacteria with different treatment. Analysis of the ratio of live to dead (B) *P. aeruginosa* and (C) *S. aureus*. (D) SEM photo of bacteria treated with AC@APTES-TA-CPBA-FeOOH with/without light.

capture of planktonic bacteria, thereby decreasing the distance between reactive oxygen species (•OH) and the bacteria, which enhances the bactericidal efficiency. The selective binding of CPBA to bacterial cell walls is attributed to the presence of these diols in the cell wall components. The boronic acid groups in CPBA can form stable complexes with the cis-diols, which are commonly found in the polysaccharide chains of bacterial cell walls. This interaction is highly specific and does not occur with other cellular components that lack the appropriate diol structures. The binding of CPBA to bacterial cell walls not only facilitates the initial adsorption of bacteria to the artificial cornea surface but also increases the local concentration of bacteria at the surface. This concentration effect enhances the efficiency of the subsequent photocatalytic disinfection by FeOOH, as the generated reactive oxygen species (ROS) can more effectively interact with the bacteria. The specific interaction between CPBA and bacterial cell walls is crucial for the antimicrobial activity of our coating. By targeting the cell wall, CPBA weakens the bacterial structure, making it more susceptible to the oxidative stress induced by the photocatalytic activity of FeOOH under light exposure. Under light conditions, the photocatalytic activity of the FeOOH component is activated, promoting the decomposition of H_2O_2 and generating a substantial quantity of reactive oxygen species. These radicals are highly effective at disrupting bacterial cell structures, leading to bacterial death.

In summary, the AC@APTES-TA-CPBA-FeOOH on artificial corneas demonstrates exceptional antibacterial performance under illuminated conditions, which is significant for enhancing the safety and efficacy of artificial corneas in clinical applications. This study underscores the potential of integrating photocatalytic materials into AC to create surfaces that are not only biocompatible but also actively antimicrobial when exposed to light, thereby offering a promising strategy for infection control in ocular prosthetics

https://doi.org/10.1021/acsomega.4c08700
ACS Omega 2025, 10, 3676−3690

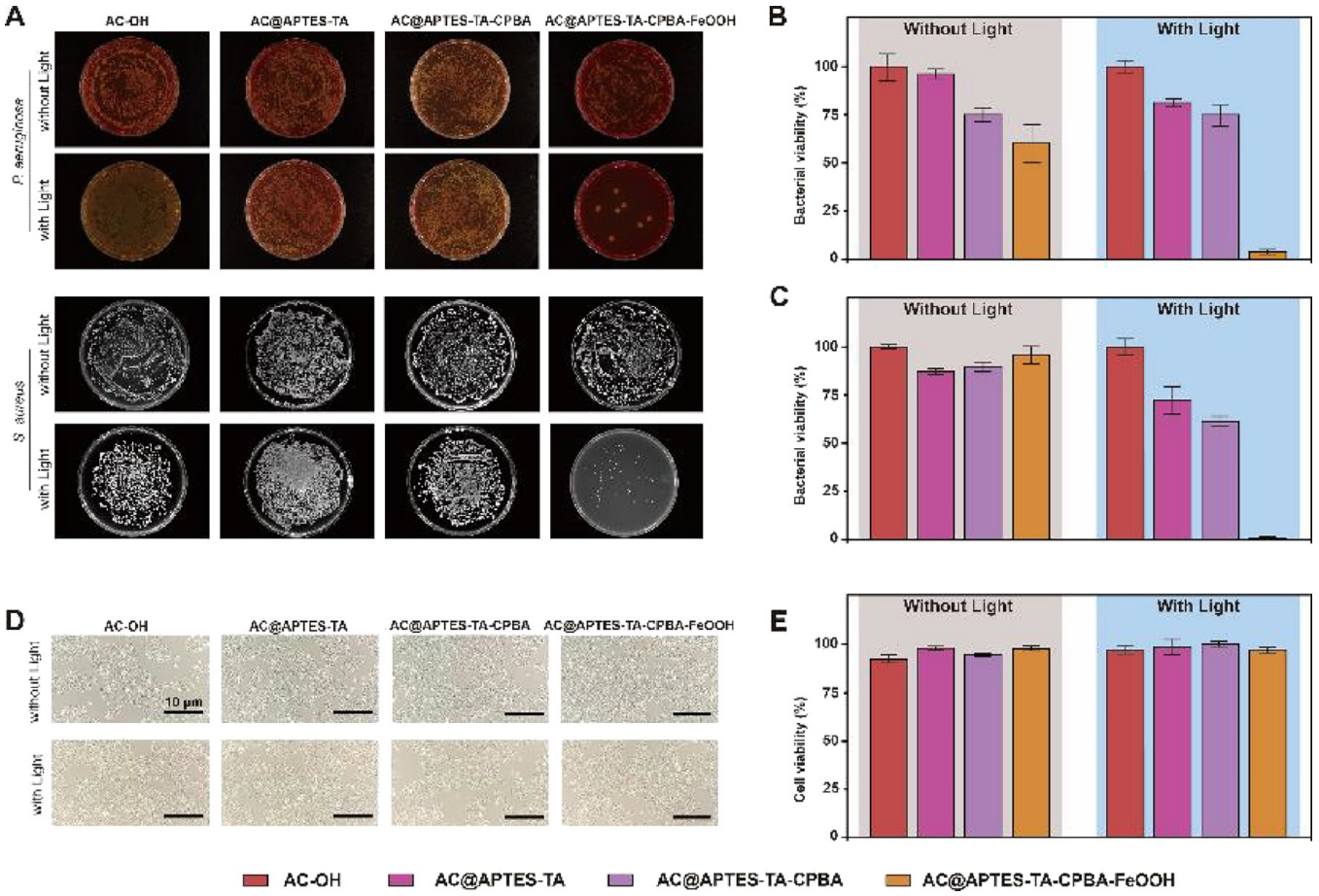

Figure 6. (A) Digital photos of bacterial agar plates with different treatments. Analysis of the bacterial viability of (B) *P. aeruginosa* and (C) *S. aureus*. (D) Digital photos of corneal epithelial cells with different treatment. (E) Cytotoxicity of AC−OH, AC@APTES-TA, AC@APTES-TA-CPBA, and AC@APTES-TA-CPBA-FeOOH with/without light.

3.6. Cytotoxicity of AC@APTES-TA-CPBA-FeOOH. In evaluating the biocompatibility of variously modified artificial corneas, namely AC−OH, AC@APTES-TA, AC@APTES-TA-CPBA, and AC@APTES-TA-CPBA-FeOOH, all demonstrated excellent biocompatibility under both illuminated and dark conditions. We confirmed that these artificial corneas exhibited no cytotoxic effects during operation, indicating no adverse impact on the growth and survival of normal cells. This exemplary biocompatibility can be attributed to the targeted action mechanism within the artificial cornea modification system (Figure 6D and 6E).

Particularly, the introduction of CPBA groups provided the artificial corneas with a specific targeting functionality capable of selectively capturing planktonic bacteria. This targeting not only enhanced the efficiency of bacterial killing but also minimized the potential side effects of reactive •OH on surrounding normal cells by shortening the trajectory of these radicals. This means that under the same operational time and intensity, the oxidative stress damage to normal cells is reduced, thus preserving cell vitality and function.

In summary, through carefully designed surface modifications, the artificial corneas are not only capable of effectively killing bacteria and enhancing their antimicrobial performance but also maintain high biocompatibility with normal cells. This balance is crucial for the clinical application of artificial corneas and the long-term health of patients, highlighting the significance of integrating advanced biomaterial technologies in ocular prosthetics. This approach ensures that while proactive measures are taken to prevent infections, cellular health within the ocular environment is not compromised, supporting overall ocular health and patient wellbeing

3.7. In Vivo Experiments. In our *in vivo* studies, we explored the potential of artificial corneas as the first reported antimicrobial corneal implants. Results indicated that unmodified artificial corneas (AC−OH group) swiftly exhibited severe signs of infection upon exposure to *Pseudomonas aeruginosa*, characterized by a milky opacity and loss of inherent transparency (Figure 7A and 7B). Similarly, mice with the unmodified AC@APTES-TA implants also suffered severe infections.

However, a significant reduction in infection severity was observed with the introduction of CPBA modifications. The AC@APTES-TA-CPBA group exhibited only mild cloudiness, with most areas of the cornea remaining clear. Further, in situ mineralization of the artificial cornea surfaces led to additional alleviation of infection, with even fewer areas of cloudiness observed. Most notably, the AC@APTES-TA-CPBA-FeOOH group exposed to light showed no signs of bacterial infection, maintaining clear and transparent corneas throughout the study.

Over time, by the third day, the infection symptoms in the AC−OH group worsened, leading to hypopyon formation and almost complete loss of vision in the mice. In contrast, while the AC@APTES-TA group did experience severe infection, it

https://doi.org/10.1021/acsomega.4c08700
ACS Omega 2025, 10, 3676−3690

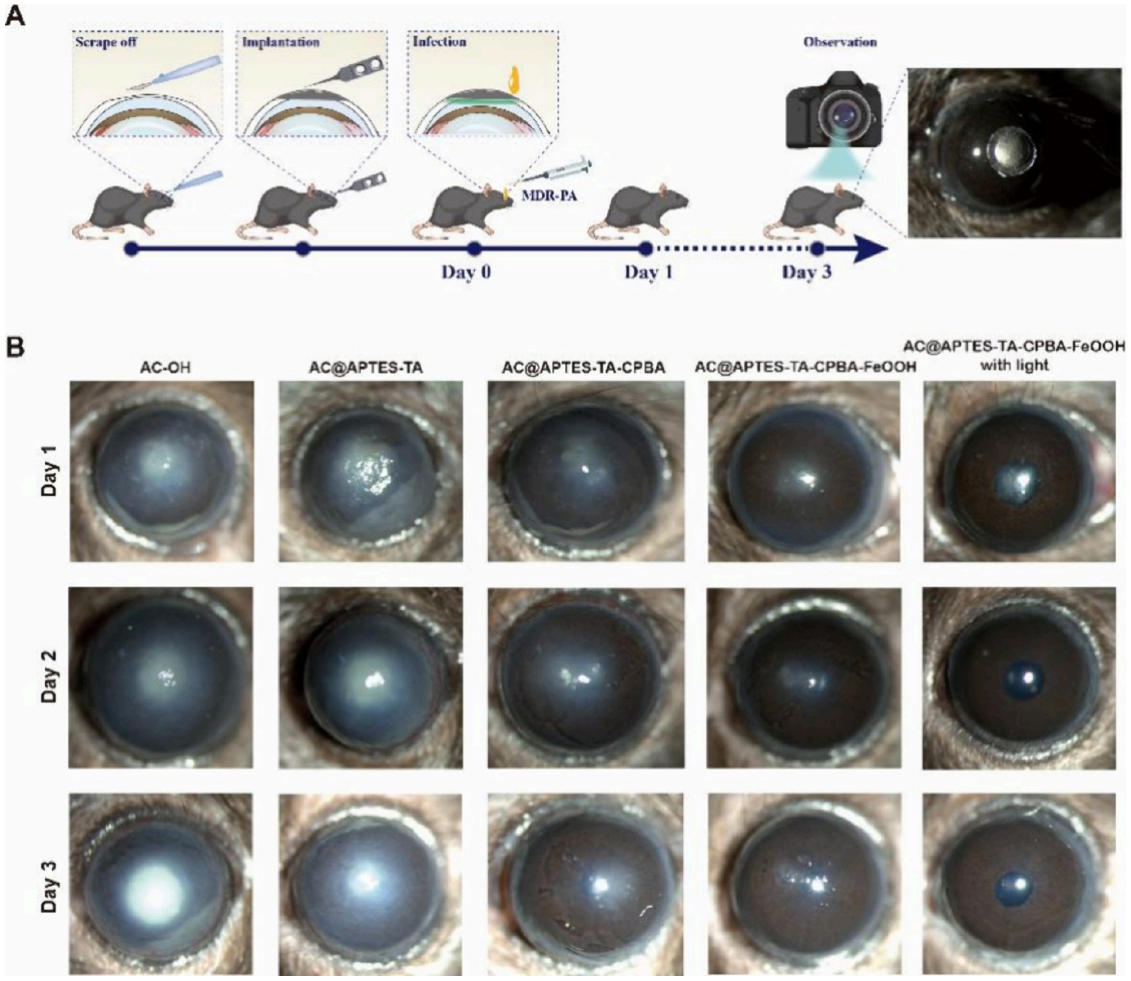

Figure 7. (A) Schematic illustration of *in vivo* antibacterial experiment of AC@APTES-TA- CPBA-FeOOH. (B) Digital photos of corneal after bacterial infection under different treatments.

did not progress to hypopyon formation. The AC@ APTES-TA-CPBA and AC@ APTES-TA-CPBA-FeOOH groups showed a self-healing trend over the three-day observation period, with conditions improving from day one and corneas nearing a transparent state. Throughout the experiment, the corneas of the AC@ APTES-TA-CPBA-FeOOH with light group remained clear and transparent.

These results reveal the inability of artificial corneas without antimicrobial modification (AC−OH and AC@ APTES-TA) to inhibit bacterial invasion. When bacterial inoculum contacted the ocular surface of the mice, bacteria quickly penetrated the gaps between the cornea and the ocular surface, entering any abrasions and causing deep infections. In contrast, artificial corneas modified with CPBA and subsequent in situ mineralization (AC@ APTES-TA-CPBA and AC@ APTES-TA- CPBA-FeOOH) demonstrated effective bacterial-targeting adsorption properties, significantly limiting the invasion by *P. aeruginosa* and substantially slowing the progression of infection. Ultimately, light activation of the mineralized surfaces triggered the photo-Fenton effect, generating a substantial amount of ROS that effectively killed the adsorbed bacteria, thereby protecting the cornea from infection. This highlights the profound impact of integrating targeted antimicrobial features and photocatalytic capabilities in artificial corneas for enhanced clinical outcomes.

3.8. Immunohistochemical Analysis. Immunohistochemical analysis of the cornea provided conclusive evidence to further validate the antimicrobial properties of specially modified artificial corneas. On the third day of the experiment, mouse corneal tissues were homogenized, and spread plate assays were performed to assess the bacterial infection status. As depicted in Figure 8A, the unmodified AC−OH group and the minimally treated AC@APTES-TA group exhibited the highest bacterial survival rates, at 100% and 90% respectively. In contrast, the bacterial survival rate within the corneas of the AC@ APTES-TA-CPBA group significantly reduced to 25%. Notably, the corneas of the in situ mineralized AC@APTES-TA-CPBA-FeOOH group and the light-exposed AC@ APTES-TA- CPBA-FeOOH with light group showed nearly undetectable levels of bacterial infection, with infection rates of 5% and 0% respectively. These findings are consistent with observations of the degree of corneal inflammatory infiltration (Figure 8B). The most severe inflammatory infiltration was observed in the AC−OH and AC@ APTES-TA groups. The degree of inflammation in the AC@ APTES-TA-CPBA group decreased to 40%, and further reduced to 20% in the AC@ APTES-TA-CPBA-FeOOH group. Particularly, in the AC@ APTES-TA-CPBA-FeOOH with light group, almost all inflammatory factors were eliminated from the cornea, with an inflammatory infiltration level of 0%.

https://doi.org/10.1021/acsomega.4c08700
ACS Omega 2025, 10, 3676−3690

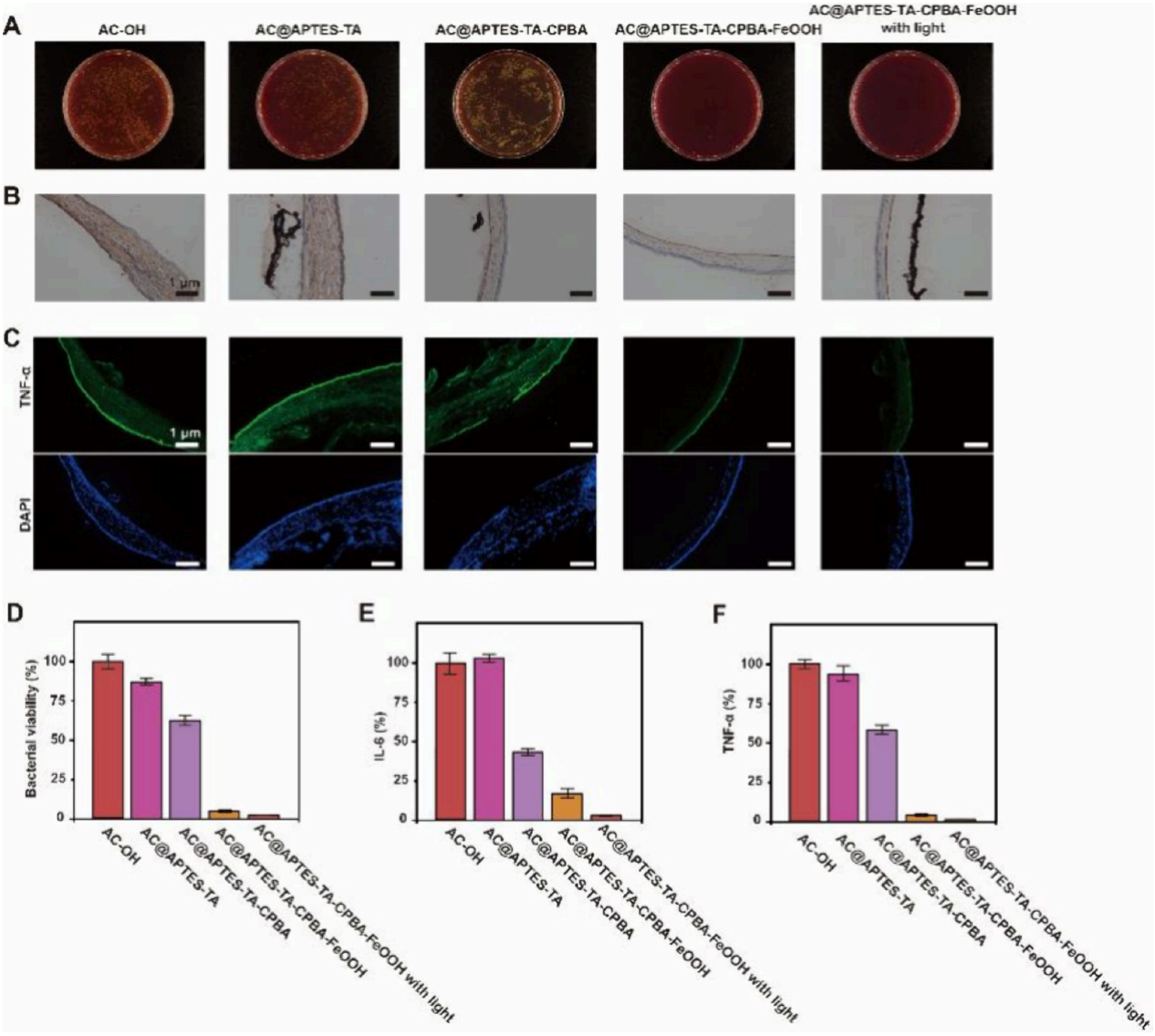

Figure 8. (A) Digital photos of bacterial agar plates, (B) immunohistochemistry staining photos, and (C) TNF-α fluorescence localization photos of mouse corneal tissue with different treatment. (D), (E), and (F) Relative analysis.

Results from the immunofluorescence experiments also aligned with these observations (refer to Figure 8C), where the distribution patterns of TNF-α within the mouse corneas closely correlated with the extent of inflammatory infiltration. Additionally, the bacterial survival rates (Figure 8D), inflammatory infiltration (Figure 8E), and distribution of TNF-α (Figure 8F) all demonstrated that under light conditions, AC@ APTES-TA-CPBA-FeOOH exhibited exceptional ability in suppressing bacterial invasion. The low bacterial survival rates and inflammatory responses achieved through AC@ APTES-TA-CPBA-FeOOH treatment under light exposure mark a significant breakthrough in the design of artificial corneal implants. This discovery not only provides new directions for the clinical application of artificial corneas but could also significantly impact future therapeutic strategies for corneal implant surgery, offering safer and more effective treatment options for patients with corneal diseases.

4. CONCLUSION

The research on the AC@ APTES-TA-CPBA-FeOOH for artificial corneas has yielded promising results, demonstrating substantial improvements in antimicrobial efficacy, biocompatibility, and *in vivo* performance, making it a potential game-changer in ocular prosthetics. The modified artificial corneas exhibited significant antimicrobial properties, particularly under light exposure, where the incorporation of CPBA and in situ mineralization with FeOOH nanoparticles dramatically enhanced bactericidal capabilities. Notably, under illuminated conditions, the AC@ APTES-TA-CPBA-FeOOH coating achieved nearly complete eradication of bacteria, showcasing the effectiveness of the photocatalytic and photo-Fenton reactions. Cytotoxicity assays confirmed that these coatings were nontoxic to normal cells, maintaining high cell viability and showing no adverse effects on cell proliferation, indicating that the modifications effectively target microbial threats while preserving the integrity of surrounding ocular tissues. *In vivo* experiments further validated the superior performance of the modified coatings, as mice implanted with these corneas

https://doi.org/10.1021/acsomega.4c08700
ACS Omega 2025, 10, 3676−3690

displayed minimal signs of infection and inflammation, particularly those treated under light conditions, where inflammatory infiltration was virtually nonexistent. Immunohistochemical analysis aligned with these results, showing reduced levels of inflammatory markers such as IL-6, suggesting that the coating's active properties prevent microbial colonization and mitigate inflammatory responses. The integration of APTES-TA, CPBA, and FeOOH into the surface coating of artificial corneas provides a multifunctional approach that enhances antimicrobial activity while ensuring biocompatibility and reducing inflammatory responses. This innovative treatment offers a promising solution to the risks associated with corneal implants, particularly infections and inflammation, thereby potentially revolutionizing the field of ophthalmic prosthetics. The findings from this study pave the way for future clinical trials and the eventual clinical application of AC@ APTES-TA-CPBA-FeOOH coated artificial corneas, aiming to improve patient outcomes in corneal transplantation and rehabilitation.

■ ASSOCIATED CONTENT

Data Availability Statement

No data was used for the research described in the article.

Supporting Information

The Supporting Information is available free of charge at https://pubs.acs.org/doi/10.1021/acsomega.4c08700.

Zeta potential, infrared spectroscopy, SEM of APTES-TA-CPBA, ultraviolet absorption spectroscopy (PDF)

■ AUTHOR INFORMATION

Corresponding Authors

Muchen Dong − *Eye Institute of Shandong First Medical University, Eye Hospital of Shandong First Medical University (Shandong Eye Hospital), Jinan, Shandong 250021, China; School of Ophthalmology, Shandong First Medical University, Jinan, Shandong 250000, China;* orcid.org/0009-0008-3435-6570; Email: dongmuchen1988@163.com

Weiyun Shi − *Eye Institute of Shandong First Medical University, Eye Hospital of Shandong First Medical University (Shandong Eye Hospital), Jinan, Shandong 250021, China; School of Ophthalmology, Shandong First Medical University, Jinan, Shandong 250000, China;* Email: weiyunshi@163.com

Authors

Qingdong Bao − *Eye Institute of Shandong First Medical University, Eye Hospital of Shandong First Medical University (Shandong Eye Hospital), Jinan, Shandong 250021, China; School of Ophthalmology, Shandong First Medical University, Jinan, Shandong 250000, China*

Ruyu Feng − *School of Ophthalmology, Shandong First Medical University, Jinan, Shandong 250000, China*

Suxia Li − *Eye Institute of Shandong First Medical University, Eye Hospital of Shandong First Medical University (Shandong Eye Hospital), Jinan, Shandong 250021, China; School of Ophthalmology, Shandong First Medical University, Jinan, Shandong 250000, China*

Xin Wang − *Eye Institute of Shandong First Medical University, Eye Hospital of Shandong First Medical University (Shandong Eye Hospital), Jinan, Shandong 250021, China; School of Ophthalmology, Shandong First Medical University, Jinan, Shandong 250000, China*

Chunxiao Dong − *Eye Institute of Shandong First Medical University, Eye Hospital of Shandong First Medical University (Shandong Eye Hospital), Jinan, Shandong 250021, China; School of Ophthalmology, Shandong First Medical University, Jinan, Shandong 250000, China*

Guangwei Li − *Eye Institute of Shandong First Medical University, Eye Hospital of Shandong First Medical University (Shandong Eye Hospital), Jinan, Shandong 250021, China; School of Ophthalmology, Shandong First Medical University, Jinan, Shandong 250000, China*

Complete contact information is available at: https://pubs.acs.org/10.1021/acsomega.4c08700

Author Contributions

#M.D. and Q.B. contributed equally to this article.

Author Contributions

M.D. and Q.B.: conceptualization, methodology, data curation, writing (original draft), writing (review and editing). R.F. and S.L.: conceptualization, methodology, writing (original draft). X.W., C.D., G.L.: conceptualization, methodology. W.S.: conceptualization, resources, writing (review and editing), visualization, supervision, project administration, funding acquisition. All authors have read and agreed to the published version of the manuscript.

Funding

This work was financially supported by National Natural Science Foundation of China (82271058 and 82271059), Shandong Provincial Natural Science Foundation (ZR2020QH146), and Shandong Provincial key research and development program (2022CXGC010505).

Notes

The authors declare no competing financial interest.

■ ACKNOWLEDGMENTS

All authors acknowledge the Eye Institute of Shandong First Medical University, Eye Hospital of Shandong First Medical University (Shandong Eye Hospital), and School of Ophthalmology, Shandong First Medical University for providing instrumental facility.

■ REFERENCES

(1) Chen, M.; Ng, S. M.; Akpek, E. K.; Ahmad, S. Artificial corneas versus donor corneas for repeat corneal transplants. *Cochrane Database Syst. Rev.* **2020**, *5* (5), No. CD009561.

(2) Baumer, K. M.; Lopez, J. J.; Naidu, S. V.; Rajendran, S.; Iglesias, M. A.; Carleton, K. M.; Eisenmann, C. J.; Carter, L. R.; Shaw, B. F. Visualizing 3D imagery by mouth using candy-like models. *Sci. Adv.* **2021**, *7* (22), No. eabh0691.

(3) Lu, X.; Ru, Y.; Chu, C.; Lv, Y.; Gao, Y.; Jia, Z.; Huang, Y.; Zhang, Y.; Zhao, S. Lentivirus-mediated IL-10-expressing Bone Marrow Mesenchymal Stem Cells promote corneal allograft survival via upregulating lncRNA 003946 in a rat model of corneal allograft rejection. *Theranostics* **2020**, *10* (18), 8446−8467.

(4) Iglesias, A. I.; Mishra, A.; Vitart, V.; Bykhovskaya, Y.; Höhn, R.; Springelkamp, H.; Cuellar-Partida, G.; Gharahkhani, P.; Bailey, J. N. C.; Willoughby, C. E.; Li, X.; Yazar, S.; Nag, A.; Khawaja, A. P.; Polašek, O.; Siscovick, D.; Mitchell, P.; Tham, Y. C.; Haines, J. L.; Kearns, L. S.; Hayward, C.; Shi, Y.; van Leeuwen, E. M.; Taylor, K. D.; Bonnemaijer, P.; Rotter, J. I.; Martin, N. G.; Zeller, T.; Mills, R. A.; Souzeau, E.; Staffieri, S. E.; Jonas, J. B.; Schmidtmann, I.; Boutin, T.; Kang, J. H.; Lucas, S. E. M.; Wong, T. Y.; Beutel, M. E.; Wilson, J. F.; Uitterlinden, A. G.; Vithana, E. N.; Foster, P. J.; Hysi, P. G.; Hewitt,

A. W.; Khor, C. C.; Pasquale, L. R.; Montgomery, G. W.; Klaver, C. C. W.; Aung, T.; Pfeiffer, N.; Mackey, D. A.; Hammond, C. J.; Cheng, C. Y.; Craig, J. E.; Rabinowitz, Y. S.; Wiggs, J. L.; Burdon, K. P.; van Duijn, C. M.; MacGregor, S. Cross-ancestry genome-wide association analysis of corneal thickness strengthens link between complex and Mendelian eye diseases. *Nat. Commun.* **2018**, *9* (1), 1864.

(5) Meng, T.; Zheng, J.; Chen, M.; Zhao, Y.; Sudarjat, H.; M R, A. A.; Kulkarni, V.; Oh, Y.; Xia, S.; Ding, Z.; Han, H.; Anders, N.; Rudek, M. A.; Chow, W.; Stark, W.; Ensign, L. M.; Hanes, J.; Xu, Q. Six-month effective treatment of corneal graft rejection. *Sci. Adv.* **2023**, *9* (12), No. eadf4608.

(6) Cheng, X.; Chen, H.; Yang, F.; Hong, J.; Cheng, Y.; Hu, J. All-small-molecule supramolecular hydrogels assembled from guanosine 5′-monophosphate disodium salt and tobramycin for the treatment of bacterial keratitis. *Bioact Mater.* **2022**, *16*, 293−300.

(7) Kim, J. K.; Nam, K. Y.; Chung, I. Y.; Jeung, W. J.; Kwon, Y. H.; Park, J. M.; Han, Y. S.; Lee, J. E.; Byon, I. S.; Park, S. H.; Kim, H. W.; Park, K. Y.; Yoon, H. S.; Park, I.; Kim, H. W.; Lee, S. J. Emerging Enterococcus isolates in postoperative endophthalmitis by selection pressure of fluoroquinolones: an 11-year multicenter and experimental study. *Emerg Microbes Infect* **2020**, *9* (1), 1892−1899.

(8) Li, W.; Thian, E. S.; Wang, M.; Wang, Z.; Ren, L. Surface design for antibacterial materials: from fundamentals to advanced strategies. *Adv. Sci.* **2021**, *8* (19), No. 2100368.

(9) Wu, Z.; Chan, B.; Low, J.; Chu, J. J. H.; Hey, H. W. D.; Tay, A. Microbial resistance to nanotechnologies: An important but understudied consideration using antimicrobial nanotechnologies in orthopaedic implants. *Bioact Mater.* **2022**, *16*, 249−270.

(10) Ou, X.; Xue, B.; Lao, Y.; Wutthinitikornkit, Y.; Tian, R.; Zou, A.; Yang, L.; Wang, W.; Cao, Y.; Li, J. Structure and sequence features of mussel adhesive protein lead to its salt-tolerant adhesion ability. *Sci. Adv.* **2020**, *6* (39), No. eabb7620.

(11) Zhang, X.; Chen, G.; Yu, Y.; Sun, L.; Zhao, Y. Bioinspired Adhesive and Antibacterial Microneedles for Versatile Transdermal Drug Delivery. *Research* **2020**, *2020*, No. 3672120.

(12) Chouke, P. B.; Shrirame, T.; Potbhare, A. K.; Mondal, A.; Chaudhary, A. R.; Mondal, S.; Thakare, S. R.; Nepovimova, E.; Valis, M.; Kuca, K.; Sharma, R.; Chaudhary, R. G. Bioinspired metal/metal oxide nanoparticles: A road map to potential applications. *Materials Today Advances* **2022**, *16*, No. 100314.

(13) Sahu, R.; Ninan, N.; Nguyen, N. H.; Wang, J.; Nguyen, M. T.; Vasilev, K.; Truong, V. K.; Tang, Y. Antibacterial Plasma Coating with Aggregation-Induced Emission Photosensitizers to Prevent Surgical Site Infections. *Adv. Mater. Interfaces* **2024**, *11* (15), No. 2400053.

(14) Pham, T.; Nguyen, T. T.; Nguyen, N. H.; Hayles, A.; Li, W.; Pham, D. Q.; Nguyen, C. K.; Nguyen, T.; Vongsvivut, J.; Ninan, N.; Sabri, Y.; Zhang, W.; Vasilev, K.; Truong, V. K. Transforming Spirulina maxima Biomass into Ultrathin Bioactive Coatings Using an Atmospheric Plasma Jet: A New Approach to Healing of Infected Wounds. *Small* **2024**, *20* (39), No. 2305469.

(15) Wohlgemuth, I.; Garofalo, R.; Samatova, E.; Günenç, A. N.; Lenz, C.; Urlaub, H.; Rodnina, M. V. Translation error clusters induced by aminoglycoside antibiotics. *Nat. Commun.* **2021**, *12* (1), 1830.

(16) He, M.; Wang, Z.; Yang, H.; Wang, Q.; Xiang, D.; Pang, X.; Chan, Y. K.; Sun, D.; Yin, G.; Yang, W.; Deng, Y. Multi-Functional Bio-HJzyme: Revolutionizing Diabetic Skin Regeneration with its Glucose-Unlocked Sterilization and Programmed Anti-Inflammatory Effects. *Adv. Sci.* **2023**, *10* (21), No. 2300986.

(17) Wang, Y.; Jiao, Z.; Li, W.; Zeng, S.; Deng, J.; Wang, M.; Ren, L. Superhydrophilic membrane with photo-Fenton self-cleaning property for effective microalgae anti-fouling. *Chin. Chem. Lett.* **2023**, *34* (8), No. 108020.

(18) Song, C.; Chen, Y.; Liu, L.; Lei, H.; Yang, X.; Hu, J.; Li, Q.; Yang, Y.; Li, Y. In situ alloying Ti−Ag antibacterial biomaterials via laser powder bed fusion: Microstructure, mechanical properties and bioperformance. *Materials Today Advances* **2023**, *20*, No. 100445.

(19) Wang, L.; He, H.; Yang, X.; Zhang, Y.; Xiong, S.; Wang, C.; Yang, X.; Chen, B.; Wang, Q. Bimetallic ions regulated PEEK of bone implantation for antibacterial and osteogenic activities. *Materials Today Advances* **2021**, *12*, No. 100162.

(20) Liu, Y.; Li, S.; Lan, W.; Hossen, M. A.; Qin, W.; Lee, K. Electrospun antibacterial and antiviral poly(ε-caprolactone)/zein/Ag bead-on-string membranes and its application in air filtration. *Materials Today Advances* **2021**, *12*, No. 100173.

(21) Gulati, K. Nano- and Micro-Engineered Biomaterials: Trigger, Therapy and Toxicity Evaluations. *Materials Today Advances* **2022**, *16*, No. 100311.

(22) Li, W.; Chen, H.; Cai, J.; Wang, M.; Zhou, X.; Ren, L. Poly(pentahydropyrimidine)-Based Hybrid Hydrogel with Synergistic Antibacterial and Pro-Angiogenic Ability for the Therapy of Diabetic Foot Ulcers. *Adv. Funct. Mater.* **2023**, *33* (49), No. 2303147.

(23) Ejima, H.; Richardson, J. J.; Liang, K.; Best, J. P.; van Koeverden, M. P.; Such, G. K.; Cui, J.; Caruso, F. One-step assembly of coordination complexes for versatile film and particle engineering. *Science* **2013**, *341* (6142), 154−157.

(24) Murphy, M. P.; Bayir, H.; Belousov, V.; Chang, C. J.; Davies, K. J. A.; Davies, M. J.; Dick, T. P.; Finkel, T.; Forman, H. J.; Janssen-Heininger, Y.; Gems, D.; Kagan, V. E.; Kalyanaraman, B.; Larsson, N.-G.; Milne, G. L.; Nyström, T.; Poulsen, H. E.; Radi, R.; Van Remmen, H.; Schumacker, P. T.; Thornalley, P. J.; Toyokuni, S.; Winterbourn, C. C.; Yin, H.; Halliwell, B. Guidelines for measuring reactive oxygen species and oxidative damage in cells and in vivo. *Nature Metabolism* **2022**, *4* (6), 651−662.

(25) Kondengadan, S. M.; Wang, B Quantitative Factors Introduced in the Feasibility Analysis of Reactive Oxygen Species (ROS)-Sensitive Triggers. *Angew. Chem., Int. Ed.* **2024**, *63* (26), No. e202403880.

https://doi.org/10.1021/acsomega.4c08700
ACS Omega 2025, 10, 3676−3690